The Effects of Acute Running Induced Neuronal Activation on Cerebral GLUT1 and Vascular Plasticity

Jacky Liang

Thesis submitted to the

Faculty of Graduate and Postdoctoral Studies

in partial fulfillment of the requirements for the MSc degree in Psychology

School of Psychology

Faculty of Social Sciences

University of Ottawa

Acknowledgements

I would like to acknowledge and thank my thesis supervisor, Dr. Claude Messier, for his support, guidance, encouragement and training that allowed me to develop my research skills. I am also like to thank my family for their continued support during my years in Ottawa. Finally, I would like to thank my friends and fellow graduate students who, in a variety of ways, have supported me throughout my graduate study.

Table of Contents

Abstract

Morphologic and metabolic change is a known property of the adult brain. A number of behavioural tasks alter local cerebral blood flow and glucose utilisation. The expression of the glucose transporter 1 (GLUT1), which allows the entry of glucose to the brain, also has been shown to change in response to long-lasting neuronal activation. However, little is known about the effect of acute neuronal activation on GLUT1 expression. Using immunohistochemistry and Western blot, we investigated cerebral GLUT1 expression and vasculature density in mice undergoing a 48-hour voluntary wheel running period. The results showed that the striatum was the main region where GLUT1 protein was up-regulated: There was a trend for GLUT1 expression and blood vessels density to be associated with the distance run during the experiment. These results indicate that short-term increased neuronal activation is associated with rapid changes in glucose transport and possibly vascular remodelling.

The Effects of Acute Running Induced Neuronal Activation on the Cerebral GLUT1 and Vascular Plasticity

Glucose is the most important carbohydrate for energy storage and extraction. In mammals, glucose is brought to every cell by the circulatory system, where it is used as the primary energy source and metabolic intermediate. The brain is among the highest glucose users in the body. This thesis examines the metabolic adaptations in the mouse brain in response to an increased cerebral energy requirement associated with increased neuronal activity. More specifically, it examines the change in the vasculature and the expression of the main glucose transporter (GLUT) in the brain following a 48-hour bout of voluntary wheel running.

The main hypothesis is that running in a wheel will lead to adaptations in the brain structures associated with motor activity. The adaptations expected are an increase in GLUT1 on blood vessels and changes in the vascular structure. When neuronal energy demand increases during behavioural activities such as learning or exercising, a glucose deficit occurs. Glucose deficit can be alleviated by increasing blood flow, vessel size, or GLUT1 density to allow more glucose into the brain regions that are activated. The present hypothesis is based on two previous experiments. First, Choeiri, Staines, Miki, Seino, and Messier (2005) have shown that GLUT1 expression in the hippocampus increased following a bar pressing task. Secondly, Allen (2010) demonstrated that, following voluntary running, there is a similar GLUT1 upregulation and that blood vessel surface increases.

In the following sections, I will briefly summarize the research describing the cerebral morphologic and metabolic changes following various conditions leading to increased brain activation.

The Plastic Brain

Neuronal plasticity is the property of the individual neurons or neuronal networks to adapt their structural and functional organization in response to new situations. Early observations of this plasticity were made during developmental stage in animals including a time window, called 'critical period', during which neural circuits are extremely sensitive to experience dependent modification (Hensch, 2004). For some time, it was believed that this neuronal plasticity was lost or greatly reduced after this critical period ended, and that neuronal structure remained fixed thereafter. However, the concept of a rigidly wired adult brain was challenged by numerous studies. Accumulated data now show that lack of input or overstimulation, learning, decreased or increased usage, and injury can lead to dendrite spine, axon, and synapse formation or removal (Bavelier, Levi, Li, Dan, & Hensch, 2010; Holtmaat & Svoboda, 2009). This concept of lifelong plastic mammalian brain is now widely accepted.

Dendritic Plasticity

Dendrites are the sites where neurons receive and integrate information from axonal terminal at synapses. Along dendrites, many small protrusions can be seen under the electronic microscope. The size, shape and number of these protrusions vary during development and differ among different types of neurons (Nimchinsky, Sabatini, & Svoboda, 2002). The exact classification of these protuberances is still debated. However, protrusions

that do not form functional synapses are usually classified as filopodia. Filopodia are precursors of dendritic spines, which are defined as mature protrusions that receive synaptic contacts from nearby axons or other dendrites (Fu & Zuo, 2011; Matsuzaki, 2001). Although dendritic spines are replaced rapidly throughout development, spine structure and numbers also change during adulthood. For example, monocular deprivation increases spine formation and density in the mouse binocular region (Wilbrecht, Holtmaat, Wright, Fox, & Svoboda, 2010). Similar spine plasticity is observed in the mouse motor cortex. Xu et al. (2009), in a forelimb reaching task, have demonstrated that new spines can be observed in the motor cortex one hour after a new training task. Spine elimination is also part of spine plasticity. However, newly generated spines can persist for a long time. This suggests that new spines induced during learning are preferentially stabilized by use. Spine plasticity only occurred in previously untrained mice, and not in mice that were previously trained in the same task during adolescence Xu et al. (2009). Subsequent training of adult mice in both groups with a different motor task was also associated with spine plasticity in the motor cortex. These results suggest that each new skill training leads to changes in specific spine compartments in the motor cortex.

Axonal Plasticity

Axons and their axonal boutons transmit the output of a neuron to neuronal networks. There are two major types of axonal boutons: en passant boutons that usually form synapses with dendritic spines; and terminal boutons, which are situated at the tip of the axon generally connect to dendrite shafts (De Paola et al., 2006; McAllister, 2007). In adulthood, boutons in

different types of axons vary in morphology and amount of plasticity. For example, axons in the thalamus have relatively stable en passant boutons, whereas axons from the cortical laminar layer VI contain a higher density of terminal boutons with a high turnover rate (De Paola et al., 2006). Both kind of boutons have the ability to extent and retract, together with the malleable dendritic spines, they play a important role in synaptic formation and elimination.(Holtmaat, De Paola, Wilbrecht, & Knott, 2008).

Synaptic formation or elimination also follows structural remodelling. Marik, Yamahachi, McManus, Szabo, and Gilbert (2010) have shown in mice that selective removal of whiskers leads to a massive remodelling of axons in the barrel cortex. In that study, excitatory neurons in the deprivation barrel zone (regions corresponding to the removed whiskers) show an increase of axonal projections from non-deprived whisker associated barrels. Conversely, inhibitory neurons in deprived zones extend their axons towards non-deprived zones. This reciprocal sprouting of axons contributes to the observed changes in the sensory topographic map. Similarly, Kleim, Barbay, et al. (2002) have demonstrated that learning a new complex motor learning task requiring one hind-limb increases synaptic densities and leads to significant functional reorganization of specific receptive fields in the motor cortex.

This short summary highlights that the adult brain remains a dynamic organ with the capacity to structurally and functionally adapt in order to meet specific demands. While axons and dendrites are relatively stable in adulthood, a significant subset of synaptic structures can be modified by learning, sensory and motor experiences.

Blood Vessels Plasticity

The brain's plasticity is not limited to modifications of neuronal connectivity and morphology. Although experience-dependent changes in synaptic structure and morphology have been prominent, plastic changes of non-neuronal elements such as cerebral capillaries have also been studied.

Blood vessels play a critical role in oxygen, nutrients supply, and waste disposal in the whole body. In the human brain, magnetic resonance imaging shows increases in blood flow and volume as a rapid consequence of sensory stimulation (Kwong et al., 1992), motor activity (Kim et al., 1993) and learning (Ogawa et al., 1993). Sustained cerebral activation appears to lead to increases in capillary density and diameter. One of the earliest evidence for this occurrence was provided by Black, Sirevaag, and Greenough (1987) in the rat visual cortex. They found that, compared to individual housing animal, exposing the rodent to a more complex environment during rearing increased occipital cortex thickness, number of synaptic contacts per neuron and larger dendritic arborisation. Moreover, the number and volume of blood capillaries in rats reared in a complex environment were nearly double of that of control animals. In a complex environment, brain stimulation results from both sensory-motor activity and learning. In order to separate those contributions, Black, Isaacs, Anderson, Alcantara, and Greenough (1990) trained adult rats either to perform a complex acrobatic training demanding a substantial degree of motor leaning but little motor activity, or a repetitive physical exercises (running wheel) with less learning but more intense motor demands. They found that after 30 days of training, motor learning in the acrobatic task led to

a 25% increase in the number of synapses in Purkinje cells of the paramedian lobule cerebellar without significant changes in blood capillary density. However, wheel running increased capillary density in the cerebellar molecular layer but did not produce synaptogenesis. These results suggest that learning new skills requires neural networks remodelling whereas repeated activation of existing circuits leads to denser vasculature. Other studies have also shown that chronic motor activity enhances the formation of new blood capillaries (angiogenesis) in the motor cortex (Kleim, Cooper, & VandenBerg, 2002; Swain et al., 2003) and motor related region such as frontoparietal cortex and dorsolateral striatum (Ding et al., 2006). Together, these findings suggest that persistent exercise leads to vascular plasticity such as angiogenesis and capillary blood flow in specific motor regions of the cerebral cortex.

Metabolic Plasticity

The brain is a high-energy organ, especially in primates. In humans, the adult brain receives 15% of the cardiovascular system blood flow, it consumes more than 20% of the oxygen in the body and over 25% of all circulating glucose even though it is only 2% of the total body weight (Pellerin, 2010). Glucose is the most essential metabolic fuel of the brain, but to reach brain cells, glucose must go through the blood-brain barrier and several other cell membranes before becoming available. Glucose is transported mainly by specialized trans-membrane glucose facilitative transporters (Maher, Vannucci, & Simpson, 1994).

GLUTs are bidirectional uniporters that move their substrates down the potential gradient (Barros & Deitmer, 2010). A total of 14 isoforms of GLUTs that share common structural features have been identified (Augustin, 2010). Based on gene sequence similarity,

the extended GLUT family can be divided into three subclasses: class I comprises all four classical GLUTs 1 to 4, including GLUT14, a gene duplication of GLUT3 (Wu & Freeze, 2002); class II includes four fructose-related transporters GLUT5, 7, 9 and 11; class III contains the remaining GLUT6, 8, 10, 12 and 13 (Joost & Thorens, 2001). Only a subset of these transporters have been found in the central nervous systems: GLUT1 to 6, GLUT8 and GLUT10 (McEwen & Reagan, 2004).

Cerebral Glucose Uptake

GLUT1 is one of the major glucose transporter isoforms: it was the first GLUT to be described in the brain and periphery (Mueckler et al., 1985). Two different forms of GLUT1 have been identified in mammalian brain. Although the higher molecular weight 55 kDa GLUT1 only differs from the lower molecular weight 45 kDa isoform in the extent of glycosylation, each of them plays an unique role in the cerebral transport of glucose (Birnbaum, Haspel, & Rosen, 1986). The 55 kDa GLUT1, which is also found in red blood cells, is present in the endothelial cells that make up the blood-brain barrier. This first carrier shuttling glucose into the brain is distributed asymmetrically. Compared to the luminal membrane (the side in contact with blood), there is three to four times more 55kDa GLUT1 on the abluminal membrane (the brain side) (Farrell & Pardridge, 1991). This distribution is thought to allow a quicker delivery of sugar from a high glucose concentrated luminal side into the parenchyma where the glucose concentration is relatively lower (Choeiri, Staines, & Messier, 2002; Dobrogowska & Vorbrodt, 1999). However, as suggested by a few studies, the GLUT1 abluminal to luminal ratio can be changed, by recruiting the intracellular GLUT1,

depending on the cerebral glucose demand (Gerhart, LeVasseur, Broderius, & Drewes, 1989; Simpson et al., 1999; Simpson, Carruthers, & Vannucci, 2007). Once glucose enters the brain proper, two distribution mechanisms have been proposed : neuronal glucose uptake and astrocytes glucose uptake. Although it is generally accepted that both mechanisms are contributing to respond to cerebral energy demand, their relative importance is still subject to debate.

Neuronal Glucose Uptake

This first glucose uptake mechanism, also called the conventional pathway, is highlighted by the third isoform of the glucose transporter family. GLUT3 is expressed at high levels in neural tissue. However, GLUT3 is also expressed in tissues with high demand of glucose such as testis, spermatozoa, placenta, and some cancer cells (Augustin, 2010). In the brain, GLUT3 is exclusively found on axonal and dendritic fibres, where the energy demand is highest (Leino, Gerhart, van Bueren, McCall, & Drewes, 1997). Neurons can take up glucose transported by the 55 kDa GLUT1 from the blood circulation into the extracellular fluid surrounding brain cells.

Two insulin-sensitive GLUTs are also found on neuron cell bodies: GLUT4 and GLUT8. However, their expression is much more sparse than that of GLUT1 and GLUT3 (McEwen & Reagan, 2004). GLUT4 is found in some neurons of the hippocampus, the cerebellum and scattered at a lower level throughout the brain (Barros & Deitmer, 2010; Choeiri et al., 2002). GLUT8 has been mostly detected in neurons from hypothalamus, cerebellum and hippocampus at the intracellular organelles level, where it appears to play a

cell homeostasis role rather than one of uptake (Ibberson, Uldry, & Thorens, 2000; McEwen & Reagan, 2004). Although GLUT4 has a similar translocation response to insulin as in the peripheral GLUT4 (Grillo, Piroli, Hendry, & Reagan, 2009), it appears to have a lesser role in general neuronal glucose uptake.

Although this simple model is widely accepted, recent data put this view into question. For example, if glucose were the main energy substrate of neurons, then we would expect most of the glucose to be metabolised by neurons. However, Barros et al. (2009) has shown that the cerebellar glial cells glucose uptake is several times those of Purkinje cells. Similarly, Vega, Martiel, Drouhault, Burckhart, and Coles (2003) have shown that non-myelinating Schwann cells, the counterparts of astrocytes in the peripheral nervous system, take up approximately 78% of glucose, although neurons are thought to be the major consumer of glucose in the brain. To resolve this paradox, the fact that neurons do not uptake much of glucose despite their high energy consumption, a second cerebral glucose uptake and utilization pathway has been proposed by Pellerin and Magistretti (2003).

Astrocytes Glucose Uptake - Lactate Shuttle

Astrocytes are glial star-shaped cells that outnumber neurons by a factor of ten in some human brain areas (Pellerin, 2010). A specific glucose transporter on the membrane of astrocytes, the 45 kDa non-vascular isoform of GLUT1, provides glucose uptake for these cells. Astrocytes have a characteristic star-like shape with multiple projections, called astrocytic end-feet, which are in extensive contacts with endothelial cells from capillaries on the one hand, and cover synaptic terminals on the other hand. Astrocytes form interconnected

networks through electrical gap junctions. Astrocytic networks provide a link between synaptic activity and blood capillary functions such as vasodilatation to match nutrient uptake and neuronal activity (Haydon, 2001).

When increased neuronal activity (which is associated with increased energy requirements) occurs, astrocytes release glutamate, the main central nervous system excitatory neurotransmitter. This signal activates a cascade of molecular events in nearby astrocytes and leads to increased glucose uptake and utilization. However, astrocytes do not use all the glucose that it takes up. Rather a significant portion of the glucose is metabolized into lactate, a high-energy metabolic intermediate (Pellerin & Magistretti, 2003). Following this first step, lactate is transported by a family of symporters called monocarboxylate transporter (MCT). Lactate produced in astrocytes is released via MCT1 and MCT4 into the extracellular space where energy-demanding neurons take up lactate through MCT2 (Barros & Deitmer, 2010; Pellerin & Magistretti, 2003).

Although the lactate shuttle hypothesis resolves some problems of the conventional view of glucose uptake, this new hypothesis still has some unsolved issues. For example, in inhibitory neurons, GABA is released instead of glutamate so that the need for lactate is less important since GABA is not metabolized from glucose as glutamate is (Arthurs & Boniface, 2002). Nehlig, Wittendorp-Rechenmann, and Lam (2004), using a novel microautoradiographic imaging technique, found that glucose uptake happens in both neurons and astrocytes at a similar rate. These findings suggest that both cerebral glucose uptake paths

are used, yet, further research will needed to determine the relative weight of each transport route in the various brain regions.

Glucose Transporter Plasticity

Local cerebral glucose utilization (LCGU) has been shown to vary in parallel with region specific increased neuronal activity (Barrett, Shumake, Jones, & Gonzalez-Lima, 2003; Choeiri et al., 2005). For example, learning and memory tasks produce increases in glucose metabolism in the hippocampus and memory processing regions (Friedman & Goldman-Rakic, 1988, 1994), while running exercise raise the cerebellum LCGU the most among other brain regions associated with motor functions (Vissing, Andersen, & Diemer, 1996). Being two major glucose conveying proteins, GLUT1 and GLUT3 have also been shown to follow the LCGU changes. Duelli, Staudt, Grunwald, and Kuschinsky (1998) used one-week administration of nicotine solution to induce a chronic but localised neuronal activation; they observed that the densities of GLUT1 and GLUT3 are increased in parallel with the increase of LCGU. The same up-regulation of GLUTs in response to augmented LCGU has also been demonstrated using a different neuronal activation method, in which water deprivation was used to stimulate the osmoregulatory system of the brain (Duelli, Maurer, Heiland, Elste, & Kuschinsky, 1999; Vannucci, Maher, Koehler, & Simpson, 1994). A matching decrease of glucose uptake and glucose transporters has also been observed in a visual deprivation experiment by Duelli, Maurer, and Kuschinsky (1998).

Other studies have examined the impact of diabetes on brain glucose transporters. Diabetes leads to blood glucose increases that are matched by increased brain glucose levels

even though brain levels of glucose remain at about 30% of those of the blood levels. However, results obtained from diabetic models (mostly the streptozotocin toxic model) are indecisive (McEwen & Reagan, 2004). There are only two convincing demonstrations of *in vivo* glucose transporter plasticity in response to increased neuronal activity. A first one was provided by Choeiri et al. (2005). They found that mouse 45 kDa GLUT1 immunoreactivity level in the hippocampus CA1 and in the sensorimotor cortex was increased following one session of operant conditioning training. A follow-up study by Allen (2010) showed increased GLUT1 immunoreactivity in the motor cortex following 48h of wheel running exercise.

The present experiment used a simple 48 hours free access to a running wheel access as a means of neuronal activation in mouse. The cerebral GLUT1 expression and vasculature density was be examined. We hypothesized that the GLUT1 expression and blood vessel density would undergo plastic changes in motor regions of the brain as a response to an increased neuronal energy demand associated with the new wheel running behaviour.

Method

Animals and Running Task

Male CD1 mice (Charles River, Canada), 8 to 10 weeks old, were used. Upon arrival to the animal facility, animals were maintained in standard individual cages (28 x 18 x 12 cm) for 7 days on a 12-h day-night cycle (7 am to 7 pm) with unrestricted access to food and water. To allow the installation of the running wheel, all mice were transferred to a bigger cage (45 x 26 x 22 cm). Animals in the control group (n=34) were housed in standard-sized cages without a running wheel. Sham animals (n=30) had access to a non-operational wheel for 48

hours to control for the effects of environmental novelty. The experimental group (n=40) had free access to a running wheel for 48 hours. The distance run by the experimental animals was recorded with a dB2L cycle computer (FILZER Enterprises Inc., USA) fitted to each wheel. Plastic running wheels had a diameter of 11.5 cm and were purchased at a local pet store. All experiments conformed to and were approved by the Animal Care Protocol Review Committee of the University of Ottawa and followed the guidelines of the Canadian Council on Animal Care on the ethical use of animals.

Tissue Preparation

A subset of mice in each group was selected for immunohistochemistry (control n=12, sham n=13, experimental n=22). The remaining brain tissues (control n=22, sham n=17, experimental n=18) were collected for Western blot analysis.

Immunohistochemistry. Animals were anaesthetized by an intraperitoneal injection of pentobarbital (65mg/kg) and perfused transcardially with 20 ml of saline followed by 20 ml of Lana's fixative (4% paraformaldehyde, 0.2% picric acid in 0.16M sodium phosphate buffer, pH 7.1). The brain was extracted and post-fixed for one hour at 4^{o}C. The brain was then transferred to a 10% sucrose in 0.1M sodium phosphate buffer, pH 7.1, for cryoprotection. The sucrose solution was changed three times over a 20-hour period before freezing the brain with CO_2. Frozen sagittal sections (14μm) were cut using a cryostat and transferred onto positively charged glass slides (Superfrost Plus, Fisher Scientific, Ottawa, ON, Canada) and stored at -80 ^{o}C.

Western Blot. Animals were anaesthetized as described earlier and perfused transcardially with 20 ml of saline to remove blood. Motor-related structures including the motor and primary somatosensory cortices, striatum, and cerebellum (brain tissue were sampled along the primary fissure of each hemisphere including the cerebellar vermis).

The visual cortex and whole hippocampus were collected as control regions. Tissue was immediately frozen on dry ice, and samples were stored at -80 °C. Brain tissue was homogenized in a manual homogenizer in Tris–HCl (10 mM Tris–HCl, 0.1 mM EDTA, pH 7.5) containing a protease inhibitor cocktail (dilution 1:50, Sigma-Aldrich Canada limited, Oakville, ON, Canada). Homogenates were centrifuged at 500xg for 10 minutes. The resulting supernatant was centrifuged at 48000xg for 10 min. The pellet was washed with 100 µl of Tris–HCl protease inhibitor cocktail and re-centrifuged at 48,000g for 10 min. Finally, the resulting pellet was re-suspended in Tris–HCl buffer and protein quantification was carried out using a standardized bovine serum albumin (BSA) kit (Pierce, Rockford, IL, USA).

Immunohistochemistry

Sections were rinsed in phosphate-buffered saline (PBS) (10mM phosphate, 0.9% saline) for a few minutes followed by incubation for three hours at room temperature with a rabbit anti-GLUT1 (dilution 1:1000, Millipore Corporation, Temecula, CA, USA) and a goat anti-CD31 (dilution 1:1000, Santa Cruz Biotechnology, Santa Cruz, CA, USA) antibody, diluted using 0.3% Triton X-100 in PBS. Tissue sections were washed (3 x 5 minutes) in PBS, then incubated with an Alexa 488 donkey anti-rabbit (dilution 1:1000, Molecular Probes corporation, Invitrogen, Burlington, ON, Canada) and an Alexa594 donkey anti-goat (dilution

1:1000, Molecular Probes corporation, Invitrogen, Burlington, ON, Canada) diluted with 0.3% Triton X-100 in PBS. Following incubation, sections were washed (3 x 5 minutes) in PBS and coverslipped using a non-commercial antifade solution (50mg p-phenylamine diamine in glycerol, pH 8.0). Control experiments confirmed the specificity of the primary and secondary antibodies and the absence of artefacts.

Black and white 16 bit pictures of the sections were taken using a ProgRes Jenoptik MF Scan Digital camera and software attached to an Olympus BX51 microscope using 10x objective (Olympus Universal Plan Apochromatic and Flat Field correction objective 10X/0.40). Exposure times were 39 milliseconds and 304 milliseconds for GLUT1 and CD31 respectively. Pictures of the following structures were taken for each animal: hippocampal CA1, CA2, dentate gyrus, motor cortex, visual cortex, striatum and cerebellum. Figure 1 (Franklin and Paxinos, 2007) illustrates boxes representing the regional location where the images were taken.

Western Blot

Brain proteins were loaded at a concentration of 100 µg/ml and were subjected to electrophoresis in 10% SDS PAGE polyacrylamide gel using Mini-PROTEAN 3 Dodeca Cell system (Bio-Rad Laboratories, Mississauga, ON, Canada). Proteins were transferred onto 0.2 µm nitrocellulose membranes with Trans-Blot Cell system (Bio-Rad Laboratories, Mississauga, ON, Canada). The nitrocellulose membranes were then blocked by incubation in 5% skim milk in 10mM PBS for one hour at room temperature. Blocked membranes were followed by overnight incubation at 4°C in a rabbit anti-GLUT1 (dilution 1:10000, Millipore

Corporation, Temecula, CA, USA), a mouse anti-β-tubulin (dilution 1:500, obtained from Dr. W. Staines, University of Ottawa, Ottawa, ON, Canada) and a mouse anti β-actin (dilution 1:5000, Sigma-Aldrich Canada limited, Oakville, ON, Canada) antibodies' mix diluted in 5% skim milk Tris-Buffered Saline and Tween 20 (TBST) (10 mM Tris–HCl, 150 mM NaCl, 0.1% Tween 20, pH 7.6). The following day, after 3 10-minute washes in TBST, membranes were subjected to a three hour incubation at room temperature with Alexa 680 goat anti-rabbit (dilution 1:10000, Molecular Probes corporation, Invitrogen, Burlington, ON, Canada) and IRDye 800CW donkey anti-mouse (dilution 1:10000, LI-COR Biosciences, Lincoln, NE, USA) secondary antibodies diluted in 5% skim milk TBST. Finally, membranes were washed for 3 10-minute periods in TBST, followed by one quick rinse in 10mM PBS before being scanned using an Odyssey infrared imaging system (LI-COR Biosciences, Lincoln, NE, USA). Figures 2 and 3 shows a sample membrane scanned in IR 700 and IR 800 respectively.

In order to control for protein loading error and SDS-PAGE gel variations, duplicates of each sample were loaded on each gel in a randomly determined position, and the experiment was replicated, which resulted in four measures for each sample.

Data Analysis

Immunohistochemistry. Images of immunohistochemistry were analysed using ImageJ (version 1.43u, Wayne Rasband, National Institute of Health, United States). A thresholding technique was used to measure the mean grey value (optical intensity of the labelling) and the percentage of the surface area labelled by the protein of interest. Thresholding is an analysis method that segments an image into areas that have some feature

of interest (in this case, blood vessels with GLUT1 and CD31 immunohistochemistry staining). This can be done using two approaches. The first one is to manually adjust the threshold to obtain a reasonable selection of stained blood vessels. However, this method is subjective and time consuming. The second method which uses a threshold algorithm was adopted in this study. Briefly, each image set of a brain region is thresholded using ImageJ threshold algorithms. These algorithms, using each image's optical characteristic, compute a threshold level score. This number represents a certain grey level that allows the software to divide all pixels of the image into two groups: "selected" and "not selected". In other words, the algorithm converts the original greyscale image into a binary image by setting all pixels with a grey value lower than the threshold level to zero (not selected) and all values above the threshold level to one (selected). In general, higher grey value pixels correspond to the immunohistochemistry labelling. Subsequently, all pixels that are given the value of one are restored their original grey value in order to compute the mean grey value (calculated by dividing the sum of the gray values of all the pixels in the selection by the total number of pixels of the selection) and percentage of the area stained (the percentage of the pixels that are selected by the threshold algorithm) (Diniz, 2010).

There are a great number of threshold algorithms that can be applied through ImageJ (Sezgin & Sankur, 2004). In order to choose the most appropriate selection method for each brain region, samples of 16 different algorithms were applied to one image from each brain region, and the algorithms that gave the most consistent result across regions were selected. Li's minimum cross entropy (Li & Tam, 1998) thresholding procedure provided the best solution for most regions except in the case of the cerebellum. Figure 4 illustrates the results

of various algorithms on a picture of hippocampal CA1. Yen's multilevel thresholding (Yen, Chang, & Chang, 1995) algorithm was used for the cerebellum (figure 5). Since there is good a-priori evidence that the vascularisation distribution can differ across structures imaged (making a structural comparison uninformative), using more than one measurement algorithm should not bias the analysis.

In order to control for immunolabelling variations across slides, the mean grey level of the background, which was defined as the mean grey level of 50% of the pixels with the lowest brightness, was measured. The final immunolabelling mean grey levels were calculated by subtracting the mean gray level of background from the mean gray level of objects of interest. This value represented an unbiased estimate of GLUT1 or CD31 density in the selected brain areas and was used to test the hypothesis that exercise increased the density of the GLUT1 glucose transporter. The percentage of area labelled was calculated for each structure and each protein (GLUT1 and CD31). This measure was used to provide an estimate of blood vessel density and/or size and test the hypothesis that exercise increased blood vessel size and or density.

A total of 28 separate analyses of variance were performed with experimental groups as a factor. The analyses were conducted for seven regions of interest stained for either GLUT1 or CD31 using two measures: mean grey value after subtracting the background, and percentage of area labelled. Separate one-way independent ANOVAs were used for each structure because the wide differences of blood vessel size and distribution rendered the comparison across structure meaningless. Similarly, GLUT1 and CD31 measures were not

entered as a factor because they use different primary and secondary antibodies that differ in characteristics sufficiently to render meaningless any statistical comparisons.

Blood Vessel Diameter and Density. We also measured blood vessel diameter in the striatum of 31 animals (control n=9; sham n=8; experimental n=14) using CD31 immunostaining. Blood vessels measured were sectioned along the lumen rather than across. It was found that measuring blood vessel diameters using vessels cut across the lumen would introduce a lot of uncertainty as to whether the blood vessel was cut at an angle, thus increasing diameter. Very small vessels were not measured due to light convolution (interference from out of focus light), which rendered an accurate measurement impossible. Really large vessels were also omitted because it was assumed that they would not show much change. Figure 6 (Franklin and Paxinos, 2007) presents the striatal areas where the measurements were taken under a 20X objective.

The total number of blood vessels was also counted in same striatal regions. All blood vessel branches were included, for example, a "Y" shaped branch was counted as two blood vessels. One-way independent ANOVAs were performed with one three levels of the grouping variable: control, sham, and experimental group.

Western Blot. Scans of Western Blot were analysed with Odyssey infrared imaging application software (version 3.0.21, LI-COR Biosciences, Lincoln, NE, USA). Each sample's integrated intensity was measured. Integrated intensity was used as the quantification measure because by using a uniform background that is specific to each membrane, the integrated intensity is independent of both the size of a feature drawn on the image and the resolution.

Integrated intensity measure takes into account the background intensity by subtracting it, and this intensity measurement is proportional to the amount of antibody labelling on the membrane, which allows for the control of the variability across membranes.

The integrated intensity raw measures of each of the 54 samples (six brain regions X three groups X three labelled antibodies) were plotted on a box plot. Outliers excluded from the analysis were identified by being at least 1.5 times outside of the interquartile range. Following this, the mean measurement of the integrated intensity of each sample was calculated.

To compare the GLUT1 and β-tubulin across groups, the mean integrated intensities were expressed as a ratio of integrated intensity associated with the GLUT1 or β-tubulin band over the integrated intensity associated with the β-actin band. Finally, the natural logarithm of the ratios was calculated in order to meet ANOVA assumptions of normality.

One-way independent ANOVAs were performed with one three of the grouping variable: control, sham, and experimental group. A total of 12 ANOVAs were performed. For each of the six brain regions, the measure of GLUT1 or β-tubulin was used as a dependent variable. GLUT1 and β-tubulin, and brain regions were not entered as factors because, as mentioned earlier, there is no a priori expectation that blood vessels and the two antigens are equally distributed across regions.

Results

Wheel Running Intensity

The average distance run by mice in the 48 hours period was 5.06 km±0.42 and ranged from 0.40 km to 10.47 km. The average running distance of mice in this experiment is in the lower range of what has been reported in other studies with average daily distance ranging from 3.5 km to 11.4 km in CD-1 mice (Atalayer & Rowland, 2011; Bednarczyk, Aumont, Decary, Bergeron, & Fernandes, 2009; Haupt & Schaefers, 2010). However, in these studies, running was measured for a much longer period, which may have resulted in higher daily distances. Two experimental mice did not run at all during our study. Their immunohistochemistry and Western blot measures were entered in the sham group.

Immunohistochemistry

Previous control experiments have shown the specificity of the immunohistochemistry reactions for the primary antibodies used. The contours of blood vessels in the immunohistochemistry photographs were determined using Li's minimum cross entropy thresholding for all regions except for that of the cerebellum in which Yen's multilevel thresholding was used. Table 1 presents the GLUT1 and CD31 mean grey value from immunohistochemistry staining for the seven brain regions of interest. These values represent estimates of the intensity of staining in the areas of the brain containing blood vessels. Table 2 presents the percentage of area selected that contained intense immunohistochemistry staining indicating the presence of blood vessels. This measure provides an estimate of the volume occupied by blood vessels. ANOVAs indicated that there was no overall significant difference

between groups for the staining intensity or for the percentage of area measures. Because previous studies have suggested that the amount of running may be an important variable to observe running-related changes in the brain, we also conducted a series of correlations between the distance run during the 48-hour and immunohistological measures. These values are shown in Table 3.

Table 3 presents Pearson correlations between the mean grey value of the protein of interest (GLUT1 or CD31) and the total distance run by the experimental animals. A significant negative two-tailed correlation was found at the striatum ($r= -0.47$, $P < 0.05$) between the GLUT1 mean grey value and the total distance run. Non-significant negative correlations were also observed for GLUT1 in the CA2, motor cortex, visual cortex and cerebellum. There was no significant correlation between CD31 mean grey value and distance but all correlations were negative. Thus, taken at face value, increased running and the pre-supposed increased neuronal activation were associated with a decreased expression of the glucose GLUT1 transporter. Because CD31 is expressed in endothelial cells, the present results also suggest that increased running was associated with decreased endothelial function. This is in contrast with studies showing that CD31 is upregulated by exercise in animals with brain infarct (Hu et al., 2010) and that CD31 upregulation is usually interpreted as an increase in the density of blood vessels.

To determine if there was an association between distance run and an increase in blood vessel density, we computed Pearson correlations between distance and the mean percentage of picture area containing GLUT1 or CD31 labeled area. Increased labeled area

could be interpreted either as showing more blood vessels or bigger blood vessels. Table 4 shows that, in general, increased running was associated with an increase in the area labeled with GLUT1 or CD31. A significant positive two-tailed correlation was found for CD31 in the CA2 ($r= 0.44$, $P =0.046$) and striatum ($r= 0.55$, $P =0.009$) while similar but non-significant correlations were found for GLUT1 in the striatum and visual cortex. Figure 7 presents a summary of the two types of correlations.

Taken together, these correlations suggest that increased running distance is associated with a decrease in GLUT1 and CD31 expression density accompanied by an increase in the volume occupied blood vessels as estimated by the GLUT1 and CD31 immunolabelling.

Blood vessel diameter was measured in a subset of animals (control n=9, sham n=8, experimental n=14) in order to determine whether running increased blood vessel diameter in the striatum. The striatum was chosen since it had shown the highest correlation between running distance and CD31 immunolabelled area. The analysis indicated no significant difference between group ($F(2, 28)=0.605$, $p=.55$). There was also no significant correlation between running distance and blood vessel diameter ($r=0.356$, $p=.19$). Finally there was no overall group difference in blood vessel number ($F(2, 28)=0.373$, $p=.69$) or any correlation between blood vessel number and running distance ($r=-0.11$, $p=.72$).

This suggests that the size and the density of blood vessels in the striatum remains unchanged following running exercise. However, these two measures are highly variable between animals. The accuracy of diameter measurement was limited: It was very difficult to identify if the measurement represented the actual diameter of the blood vessel (figure 8).

Also, larger vessels were often flattened by fixation to a more oval or irregular shape, which interfered with their accurate measurement. Thus, only a subset of the visible vessels was sampled and this sample may not have been representative. Secondly, in an immunohistochemistry slide, which is only a very thin two-dimensional view of a whole structure, vessels distribution is very irregular. For example, a vessel that coursed in then out of the same plane was counted twice or as many times as it went through the same brain section. These problems may be behind the conflicting results between labelling area and the measured vessel diameter and number.

Western Blot

Table 5 shows the Western blot protein quantification of GLUT1 and β-tubulin. The results of the analyses indicate a significant increase in GLUT1 protein in the hippocampus ($F(2, 53)=3.533$, $p<.05$). Tukey HSD post-hoc tests indicate a near significant difference between control and sham groups ($p=.067$), and between control and experimental groups ($p=.076$), however, the difference between sham and experimental groups are far from significant level ($p=.998$). ANOVAs also showed a significant increase in GLUT1 protein in striatum ($F(2, 45)=3.332$, $p<.05$). Tukey HSD post-hoc tests indicated a significant difference between control and experimental groups ($p=.038$). The sham group was not significantly different from other two groups. β-tubulin did not yield any significant difference between groups. Pearson's correlations between protein expression and running distance were not significant for either GLUT1 or *β*-tubulin for any of the brain regions. Contrary to immunohistochemistry results, there was no distinctive pattern observed.

Discussion

The aim of the present study was to determine if neuronal activation associated with a new motor activity would produce local upregulation in GLUT1 expression in brain regions involved in motor control such as the cerebellum, caudate nucleus and motor cortex. CD31, an endothelia cell marker, was used in order to test the hypothesis that there would also be a remodelling of capillaries in the same regions. Only a small significant increase of GLUT1 protein expression in the striatum was found but correlations between the distance run and the various measures suggested the possibility that changes were dependent on the actual physical activity.

Overall, running did not lead to changes in GLUT1 and CD31 labelling intensity or surface area. However, there was an interesting trend in Pearson's correlations between distance run and protein expression: GLUT1 and CD31 immunolabelling tended to be less intense as the animal ran a greater distance. Concurrently, the GLUT1 and CD31 labelled area tended to increase as the running distance increased. One simple explanation could be that as the exercise intensity increases, blood vessels dilated to increase blood flow in response to higher energy demand. This dilation would produce slightly larger vessels but the GLUT1 and CD31 proteins would appear less dense in the dilated vessel. Similar results have been observed in studies that explored neuronal activation following long-term exercise (Black, Zelazny, & Greenough, 1991; Kleim, Cooper, et al., 2002; Swain et al., 2003). In another experiment (Allen, 2010), the author used GLUT1 as an approximate measure of blood vessel density following 48 hours of wheel running exercise and found that running produced a significant increase in blood vessel density in all motor regions. However, in the present study,

the measure of blood vessels diameter and density in the striatum, where the highest correlation between GLUT1 and CD31 immunolabelling area was observed, did not yield any significant difference between experimental and control groups as was found. The immunolabelling results of GLUT1, as an indirect capillary measure, and CD31, a more direct vessel measurement, suggest that running exercise for 48 hours may not be long enough to observe a capillary morphology change. This is consistent with Van der Borght et al. (2009) who used GLUT1 immunostaining as a measure of blood vessel density in mice; they found increased blood vessel density in the hippocampus dentate gyrus after 72 hours but not after 24 hours of running exercise. These data suggest that cerebral GLUT1 and capillaries plasticity would occur between two and three days following exercise mediated neuronal activation.

Western blot protein quantification of *β*-tubulin did not yield any group difference contrary to a previous study (Allen, 2010), in which the author used *β*-tubulin immunolabelling as a marker of neuronal plasticity. Allen (2010) found that the cerebellum showed a strong increase in *β*-tubulin immunolabelling following two days of exercise. This disparity may due to the fact that a Western blot measurement encompasses all the tissue whereas immunohistochemistry measures are localized to the most intensely labelled areas. In other words, the small and localised *β*-tubulin change observed in immunohistochemistry may not contribute enough to the whole region measurement of the Western blot to show a significant difference. In our experiment, *β*-tubulin expression was taken as an internal protein control for the Western blot quantification. However, *β*-tubulin expression may vary following neuronal activation (Allen, 2010) presumably because the protein is incorporated in

new mature microtubules associated with developing neuronal processes (Ferreira & Caceres, 1992).

The small difference observed in the Western blot quantification of GLUT1 in the hippocampus suggests that the presence of the wheel without exercise had a small stimulatory effect. Hippocampal GLUT1 was slightly elevated in the mice using a stationary wheel compared to that of the control mice, but runners had the highest GLUT1 expression. In fact, similar small increases in GLUT1 protein were also present in the striatum and other brain regions. Although these up-regulations were not statistically significant, the trend suggests that even a short period of neuronal activation, 48 hours in this case, may be enough to cause visible change in GLUT1 distribution. This is consistent with a previous finding by Choeiri et al. (2005); GLUT1 upregulation was observed after only one session of a bar pressing operant task.

Future Direction and Limitations

Animals in the present experiment ran less, on average, compared to other studies using the same mouse strain and similar exercise wheel (Atalayer & Rowland, 2011; Bednarczyk et al., 2009; Haupt & Schaefers, 2010). Because of this, correlations between running distance and GLUT1/CD31 expression may have been reduced. Moreover, the distance run ranged from 0.40 km to 10.47 km in two days. This large variation could have limited the ability to detect significant change in protein expression. While forced running could address these issues, it is different from voluntary exercise in many respects and has been shown to be a more stressful exercise. This may explain the observed relation between

running distance and GLUT1 levels observed in a recent study using forced running (Kinni et al., 2011).

The novelty effect of the wheel introduction that was observed could also obscure potential changes in neuronal plasticity. Future studies should include pre-exposure to a non-functional running wheel for all groups prior to exercising. Voluntary exercise induced neuronal activation remains an interesting paradigm, but further optimisation is needed.

The endothelial cell specific protein CD31 is expressed in most mature endothelial cells (Carmeliet & Jain, 2011). This limited our measurements to the mature capillaries and would not have included potential immature capillaries induced by the running activity. This can be done by examine the expression of some growth factors related to exercise and angiogenesis, such as brain-derived neurotrophic factor (Donovan et al., 2000) and vascular endothelial growth factor (Carmeliet & Jain, 2011; Ding et al., 2006).

Conclusion

The present study demonstrated that a voluntary wheel running exercise for 48 hours induced an up-regulation of GLUT1 protein expression in the striatum. A trend of plastic GLUT1 expression and capillary morphology also was observed in correlation with running distance. These results support the association between the cerebral energy demand and metabolic and circulatory cerebral plasticity.

Reference

Allen, A. (2010). *The effects of running-induced neuronal activation on the plastic expression of mouse cerebral GLUTI.* M.A. dissertation, University of Ottawa (Canada), Canada, ProQuest Dissertations & Theses database. (Publication No. AAT MR65519)

Arthurs, O. J., & Boniface, S. (2002). How well do we understand the neural origins of the fMRI BOLD signal? *Trends in Neurosciences, 25*(1), 27-31. doi: 10.1016/s0166-2236(00)01995-0

Atalayer, D., & Rowland, N. E. (2011). Comparison of voluntary and foraging running wheel activity on food demand in mice. *Physiol Behav, 102*(1), 22-29. doi: S0031-9384(10)00356-2 [pii] 10.1016/j.physbeh.2010.10.003

Augustin, R. (2010). The protein family of glucose transport facilitators: It's not only about glucose after all. *IUBMB Life, 62*(5), 315-333. doi: 10.1002/iub.315

Barrett, D., Shumake, J., Jones, D., & Gonzalez-Lima, F. (2003). Metabolic mapping of mouse brain activity after extinction of a conditioned emotional response. *J Neurosci, 23*(13), 5740-5749.

Barros, L. F., Courjaret, R., Jakoby, P., Loaiza, A., Lohr, C., & Deitmer, J. W. (2009). Preferential transport and metabolism of glucose in Bergmann glia over Purkinje cells: a multiphoton study of cerebellar slices. *Glia, 57*(9), 962-970. doi: 10.1002/glia.20820

Barros, L. F., & Deitmer, J. W. (2010). Glucose and lactate supply to the synapse. *Brain Res Rev, 63*(1-2), 149-159. doi: 10.1016/j.brainresrev.2009.10.002

Bavelier, D., Levi, D. M., Li, R. W., Dan, Y., & Hensch, T. K. (2010). Removing brakes on adult brain plasticity: from molecular to behavioral interventions. *J Neurosci, 30*(45), 14964-14971. doi: 10.1523/JNEUROSCI.4812-10.2010

Bednarczyk, M. R., Aumont, A., Decary, S., Bergeron, R., & Fernandes, K. J. (2009). Prolonged voluntary wheel-running stimulates neural precursors in the hippocampus and forebrain of adult CD1 mice. *Hippocampus, 19*(10), 913-927. doi: 10.1002/hipo.20621

Birnbaum, M. J., Haspel, H. C., & Rosen, O. M. (1986). Cloning and characterization of a cDNA encoding the rat brain glucose-transporter protein. *Proc Natl Acad Sci U S A, 83*(16), 5784-5788.

Black, J. E., Isaacs, K. R., Anderson, B. J., Alcantara, A. A., & Greenough, W. T. (1990). Learning causes synaptogenesis, whereas motor activity causes angiogenesis, in cerebellar cortex of adult rats. *Proc Natl Acad Sci U S A, 87*(14), 5568-5572.

Black, J. E., Sirevaag, A. M., & Greenough, W. T. (1987). Complex experience promotes capillary formation in young rat visual cortex. *Neurosci Lett, 83*(3), 351-355.

Black, J. E., Zelazny, A. M., & Greenough, W. T. (1991). Capillary and mitochondrial support of neural plasticity in adult rat visual cortex. *Exp Neurol, 111*(2), 204-209.

Carmeliet, P., & Jain, R. K. (2011). Molecular mechanisms and clinical applications of angiogenesis. *Nature, 473*(7347), 298-307. doi: 10.1038/nature10144

Choeiri, C., Staines, W., & Messier, C. (2002). Immunohistochemical localization and quantification of glucose transporters in the mouse brain. *Neuroscience, 111*(1), 19-34. doi: S0306452201006194 [pii]

Choeiri, C., Staines, W., Miki, T., Seino, S., & Messier, C. (2005). Glucose transporter plasticity during memory processing. *Neuroscience, 130*(3), 591-600. doi: S0306-4522(04)00836-X [pii] 10.1016/j.neuroscience.2004.09.011

De Paola, V., Holtmaat, A., Knott, G., Song, S., Wilbrecht, L., Caroni, P., & Svoboda, K. (2006). Cell type-specific structural plasticity of axonal branches and boutons in the adult neocortex. *Neuron, 49*(6), 861-875. doi: S0896-6273(06)00134-6 [pii] 10.1016/j.neuron.2006.02.017

Ding, Y. H., Li, J., Zhou, Y., Rafols, J. A., Clark, J. C., & Ding, Y. (2006). Cerebral angiogenesis and expression of angiogenic factors in aging rats after exercise. *Curr Neurovasc Res, 3*(1), 15-23.

Diniz, C. (2010). Microscopic image analysis using computer-assisted methodology to quantify immunostained receptors. *Microscopy: Science, Technology, Applications and Education, 2*, 10.

Dobrogowska, D. H., & Vorbrodt, A. W. (1999). Quantitative immunocytochemical study of blood-brain barrier glucose transporter (GLUT-1) in four regions of mouse brain. *J Histochem Cytochem, 47*(8), 1021-1030.

Donovan, M. J., Lin, M. I., Wiegn, P., Ringstedt, T., Kraemer, R., Hahn, R., . . . Hempstead, B. L. (2000). Brain derived neurotrophic factor is an endothelial cell survival factor required for intramyocardial vessel stabilization. *Development, 127*(21), 4531-4540.

Duelli, R., Maurer, M. H., Heiland, S., Elste, V., & Kuschinsky, W. (1999). Brain water content, glucose transporter densities and glucose utilization after 3 days of water deprivation in the rat. *Neurosci Lett, 271*(1), 13-16. doi: S0304394099005054 [pii]

Duelli, R., Maurer, M. H., & Kuschinsky, W. (1998). Decreased glucose transporter densities, rate constants and glucose utilization in visual structures of rat brain during chronic visual deprivation. *Neurosci Lett, 250*(1), 49-52.

Duelli, R., Staudt, R., Grunwald, F., & Kuschinsky, W. (1998). Increase of glucose transporter densities (Glut1 and Glut3) during chronic administration of nicotine in rat brain. *Brain Res, 782*(1-2), 36-42.

Farrell, C. L., & Pardridge, W. M. (1991). Blood-brain barrier glucose transporter is asymmetrically distributed on brain capillary endothelial lumenal and ablumenal membranes: an electron microscopic immunogold study. *Proc Natl Acad Sci U S A, 88*(13), 5779-5783.

Ferreira, A., & Caceres, A. (1992). Expression of the class III beta-tubulin isotype in developing neurons in culture. *J Neurosci Res, 32*(4), 516-529. doi: 10.1002/jnr.490320407

Franklin, B.J. & Paxinos, G. (2007). The mouse brain in stereotaxic coordinates (3rd ed.). Elsevier.

Friedman, H. R., & Goldman-Rakic, P. S. (1988). Activation of the hippocampus and dentate gyrus by working-memory: a 2-deoxyglucose study of behaving rhesus monkeys. *J Neurosci, 8*(12), 4693-4706.

Friedman, H. R., & Goldman-Rakic, P. S. (1994). Coactivation of prefrontal cortex and inferior parietal cortex in working memory tasks revealed by 2DG functional mapping in the rhesus monkey. *J Neurosci, 14*(5 Pt 1), 2775-2788.

Fu, M., & Zuo, Y. (2011). Experience-dependent structural plasticity in the cortex. *Trends Neurosci, 34*(4), 177-187. doi: 10.1016/j.tins.2011.02.001

Gerhart, D. Z., LeVasseur, R. J., Broderius, M. A., & Drewes, L. R. (1989). Glucose transporter localization in brain using light and electron immunocytochemistry. *J Neurosci Res, 22*(4), 464-472. doi: 10.1002/jnr.490220413

Grillo, C. A., Piroli, G. G., Hendry, R. M., & Reagan, L. P. (2009). Insulin-stimulated translocation of GLUT4 to the plasma membrane in rat hippocampus is PI3-kinase dependent. *Brain Res, 1296*, 35-45. doi: 10.1016/j.brainres.2009.08.005

Haupt, M., & Schaefers, A. T. (2010). Effects of postweaning social and physical deprivation on locomotor activity patterns and explorative behavior in female CD-1 mice. *Dev Psychobiol, 52*(4), 383-393. doi: 10.1002/dev.20439

Haydon, P. G. (2001). GLIA: listening and talking to the synapse. *Nat Rev Neurosci, 2*(3), 185-193.

Hensch, T. K. (2004). Critical period regulation. *Annu Rev Neurosci, 27*, 549-579. doi: 10.1146/annurev.neuro.27.070203.144327

Holtmaat, A., De Paola, V., Wilbrecht, L., & Knott, G. W. (2008). Imaging of experience-dependent structural plasticity in the mouse neocortex in vivo. *Behav Brain Res, 192*(1), 20-25. doi: S0166-4328(08)00190-3 [pii] 10.1016/j.bbr.2008.04.005

Holtmaat, A., & Svoboda, K. (2009). Experience-dependent structural synaptic plasticity in the mammalian brain. *Nat Rev Neurosci, 10*(9), 647-658. doi: nrn2699 [pii] 10.1038/nrn2699

Hu, X., Zheng, H., Yan, T., Pan, S., Fang, J., Jiang, R., & Ma, S. (2010). Physical exercise induces expression of CD31 and facilitates neural function recovery in rats with focal cerebral infarction. *Neurol Res, 32*(4), 397-402. doi: 10.1179/016164110X12670144526309

Ibberson, M., Uldry, M., & Thorens, B. (2000). GLUTX1, a novel mammalian glucose transporter expressed in the central nervous system and insulin-sensitive tissues. *J Biol Chem, 275*(7), 4607-4612.

Joost, H. G., & Thorens, B. (2001). The extended GLUT-family of sugar/polyol transport facilitators: nomenclature, sequence characteristics, and potential function of its novel members (review). *Mol Membr Biol, 18*(4), 247-256.

Kim, S. G., Ashe, J., Hendrich, K., Ellermann, J. M., Merkle, H., Ugurbil, K., & Georgopoulos, A. P. (1993). Functional magnetic resonance imaging of motor cortex: hemispheric asymmetry and handedness. *Science, 261*(5121), 615-617.

Kinni, H., Guo, M., Ding, J. Y., Konakondla, S., Dornbos, D., 3rd, Tran, R., . . . Ding, Y. (2011). Cerebral Metabolism after Forced or Voluntary Physical Exercise. *Brain Res*. doi: S0006-8993(11)00432-X [pii] 10.1016/j.brainres.2011.02.076

Kleim, J. A., Barbay, S., Cooper, N. R., Hogg, T. M., Reidel, C. N., Remple, M. S., & Nudo, R. J. (2002). Motor learning-dependent synaptogenesis is localized to functionally reorganized motor cortex. *Neurobiol Learn Mem, 77*(1), 63-77. doi: 10.1006/nlme.2000.4004

Kleim, J. A., Cooper, N. R., & VandenBerg, P. M. (2002). Exercise induces angiogenesis but does not alter movement representations within rat motor cortex. *Brain Res, 934*(1), 1-6. doi: S0006899302022394 [pii]

Kwong, K. K., Belliveau, J. W., Chesler, D. A., Goldberg, I. E., Weisskoff, R. M., Poncelet, B. P., . . . et al. (1992). Dynamic magnetic resonance imaging of human brain activity during primary sensory stimulation. *Proc Natl Acad Sci U S A, 89*(12), 5675-5679.

Leino, R. L., Gerhart, D. Z., van Bueren, A. M., McCall, A. L., & Drewes, L. R. (1997). Ultrastructural localization of GLUT 1 and GLUT 3 glucose transporters in rat brain. *J Neurosci Res, 49*(5), 617-626. doi: 10.1002/(SICI)1097-4547(19970901)49:5<617::AID-JNR12>3.0.CO;2-S [pii]

Li, C. H., & Tam, P. K. S. (1998). An iterative algorithm for minimum cross entropy thresholding. *Pattern Recognition Letters, 19*(8), 771-776.

Maher, F., Vannucci, S. J., & Simpson, I. A. (1994). Glucose transporter proteins in brain. *FASEB J, 8*(13), 1003-1011.

Marik, S. A., Yamahachi, H., McManus, J. N., Szabo, G., & Gilbert, C. D. (2010). Axonal dynamics of excitatory and inhibitory neurons in somatosensory cortex. *PLoS Biol, 8*(6), e1000395. doi: 10.1371/journal.pbio.1000395

Matsuzaki, M. (2001). Dendritic spine geometry is critical for AMPA receptor expression in hippocampal CA1 pyramidal neurons. *Nature Neurosci., 4*, 1086-1092.

McAllister, A. K. (2007). Dynamic aspects of CNS synapse formation. *Annu Rev Neurosci, 30*, 425-450. doi: 10.1146/annurev.neuro.29.051605.112830

McEwen, B. S., & Reagan, L. P. (2004). Glucose transporter expression in the central nervous system: relationship to synaptic function. *Eur J Pharmacol, 490*(1-3), 13-24. doi: 10.1016/j.ejphar.2004.02.041

Mueckler, M., Caruso, C., Baldwin, S. A., Panico, M., Blench, I., Morris, H. R., . . . Lodish, H. F. (1985). Sequence and structure of a human glucose transporter. *Science, 229*(4717), 941-945.

Nehlig, A., Wittendorp-Rechenmann, E., & Lam, C. D. (2004). Selective uptake of [14C]2-deoxyglucose by neurons and astrocytes: high-resolution microautoradiographic imaging by cellular 14C-trajectography combined with immunohistochemistry. *J Cereb Blood Flow Metab, 24*(9), 1004-1014. doi: 10.1097/01.WCB.0000128533.84196.D8

Nimchinsky, E. A., Sabatini, B. L., & Svoboda, K. (2002). Structure and function of dendritic spines. *Annu. Rev. Physiol., 64*, 313-353.

Ogawa, S., Menon, R. S., Tank, D. W., Kim, S. G., Merkle, H., Ellermann, J. M., & Ugurbil, K. (1993). Functional brain mapping by blood oxygenation level-dependent contrast magnetic resonance imaging. A comparison of signal characteristics with a biophysical model. *Biophys J, 64*(3), 803-812. doi: 10.1016/S0006-3495(93)81441-3

Pellerin, L. (2010). Food for thought: the importance of glucose and other energy substrates for sustaining brain function under varying levels of activity. *Diabetes Metab, 36 Suppl 3*, S59-63. doi: 10.1016/S1262-3636(10)70469-9

Pellerin, L., & Magistretti, P. J. (2003). Food for thought: challenging the dogmas. *J Cereb Blood Flow Metab, 23*(11), 1282-1286. doi: 10.1097/01.WCB.0000096064.12129.3D 00004647-200311000-00003 [pii]

Sezgin, M., & Sankur, B. (2004). Survey over image thresholding techniques and quantitative performance evaluation. *Journal of Electronic Imaging, 13*(1), 146-168.

Simpson, I. A., Appel, N. M., Hokari, M., Oki, J., Holman, G. D., Maher, F., . . . Smith, Q. R. (1999). Blood-brain barrier glucose transporter: effects of hypo- and hyperglycemia revisited. *J Neurochem, 72*(1), 238-247.

Simpson, I. A., Carruthers, A., & Vannucci, S. J. (2007). Supply and demand in cerebral energy metabolism: the role of nutrient transporters. *J Cereb Blood Flow Metab, 27*(11), 1766-1791. doi: 10.1038/sj.jcbfm.9600521

Swain, R. A., Harris, A. B., Wiener, E. C., Dutka, M. V., Morris, H. D., Theien, B. E., . . . Greenough, W. T. (2003). Prolonged exercise induces angiogenesis and increases cerebral blood volume in primary motor cortex of the rat. *Neuroscience, 117*(4), 1037-1046. doi: S0306452202006644 [pii]

Van der Borght, K., Kobor-Nyakas, D. E., Klauke, K., Eggen, B. J., Nyakas, C., Van der Zee, E. A., & Meerlo, P. (2009). Physical exercise leads to rapid adaptations in hippocampal vasculature: temporal dynamics and relationship to cell proliferation and neurogenesis. *Hippocampus, 19*(10), 928-936. doi: 10.1002/hipo.20545

Vannucci, S. J., Maher, F., Koehler, E., & Simpson, I. A. (1994). Altered expression of GLUT-1 and GLUT-3 glucose transporters in neurohypophysis of water-deprived or diabetic rats. *Am J Physiol, 267*(4 Pt 1), E605-611.

Vega, C., Martiel, J. L., Drouhault, D., Burckhart, M. F., & Coles, J. A. (2003). Uptake of locally applied deoxyglucose, glucose and lactate by axons and Schwann cells of rat vagus nerve. *J Physiol, 546*(Pt 2), 551-564.

Vissing, J., Andersen, M., & Diemer, N. H. (1996). Exercise-induced changes in local cerebral glucose utilization in the rat. *J Cereb Blood Flow Metab, 16*(4), 729-736. doi: 10.1097/00004647-199607000-00025

Wilbrecht, L., Holtmaat, A., Wright, N., Fox, K., & Svoboda, K. (2010). Structural plasticity underlies experience-dependent functional plasticity of cortical circuits. *J Neurosci, 30*(14), 4927-4932. doi: 10.1523/JNEUROSCI.6403-09.2010

Wu, X., & Freeze, H. H. (2002). GLUT14, a Duplicon of GLUT3, Is Specifically Expressed in Testis as Alternative Splice Forms. *Genomics, 80*(6), 553-557. doi: 10.1006/geno.2002.7010

Xu, T., Yu, X., Perlik, A. J., Tobin, W. F., Zweig, J. A., Tennant, K., . . . Zuo, Y. (2009). Rapid formation and selective stabilization of synapses for enduring motor memories. *Nature, 462*(7275), 915-919. doi: 10.1038/nature08389

Yen, J. C., Chang, F. J., & Chang, S. (1995). A new criterion for automatic multilevel thresholding. *IEEE Trans Image Process, 4*(3), 370-378. doi: 10.1109/83.366472

Appendix

Table 1

GLUT1 and CD31 mean grey value (±S.E.M.) and F value in various brain areas.

	GLUT1				*CD31*			
Brain Region	*Control (n=12)*	*Sham (n=14)*	*Runners (n=21)*	*F*	*Control (n=12)*	*Sham (n=14)*	*Runners (n=21)*	*F*
CA1	*15116±410*	*14571±509*	*14744±485*	*0.29*	*12789±580*	*12553±396*	*12421±250*	*0.17*
CA2	*14605±409*	*14553±668*	*14564±436*	*0.01*	*12853±343*	*13110±552*	*13127±505*	*0.07*
Dentate Gyrus	*13603±725*	*13098±712*	*12234±474*	*1.39*	*12859±331*	*12212±443*	*12135±355*	*0.87*
Striatum	*13920±436*	*13250±713*	*14052±551*	*0.51*	*13973±269*	*13404±499*	*13804±450*	*0.29*
Motor Cortex	*12882±580*	*11924±480*	*12313±549*	*0.62*	*12669±401*	*12318±401*	*12489±447*	*0.10*
Visual Cortex	*12505±236*	*12307±650*	*12078±333*	*0.24*	*12068±573*	*11886±496*	*11775±449*	*0.08*
Cerebellum	*12966±399*	*12380±566*	*12651±523*	*0.24*	*11821±434*	*11829±505*	*11519±443*	*0.16*

Table 2

Mean percentage of GLUT1 and CD31 labelled area (±S.E.M.) and F value in various brain regions

Brain Region	*GLUT1*				*CD31*			
	Control (n=12)	*Sham (n=14)*	*Runners (n=21)*	*F*	*Control (n=12)*	*Sham (n=14)*	*Runners (n=21)*	*F*
CA1	*4.92±0.29*	*4.86±0.23*	*4.75±0.23*	*0.12*	*4.46±0.19*	*4.59±0.21*	*4.73±0.25*	*0.31*
CA2	*5.00±0.24*	*4.87±0.28*	*4.81±0.13*	*0.21*	*4.99±0.19*	*4.89±0.22*	*4.64±0.27*	*0.51*
Dentate Gyrus	*6.63±0.67*	*6.38±0.62*	*6.95±0.43*	*0.30*	*5.31±0.13*	*5.20±0.21*	*5.09±0.19*	*0.31*
Striatum	*6.21±0.29*	*5.94±0.39*	*6.12±0.20*	*0.20*	*5.61±0.10*	*5.54±0.34*	*5.71±0.27*	*0.10*
Motor Cortex	*6.51±0.22*	*6.46±0.33*	*6.95±0.22*	*1.20*	*6.87±0.33*	*6.72±0.26*	*6.79±0.30*	*0.04*
Visual Cortex	*6.54±0.20*	*6.18±0.30*	*6.64±0.33*	*0.57*	*7.10±0.33*	*6.92±0.31*	*6.80±0.27*	*0.25*
Cerebellum	*7.69±0.56*	*6.57±0.46*	*8.10±0.76*	*1.23*	*7.23±0.22*	*7.76±0.53*	*7.39±0.50*	*0.25*

Table 3

Correlation of GLUT1 and CD31 Immunohistochemical mean grey value and total distance run for various brain regions

Brain Region	*GLUT1 (n=21)*	*CD31 (n=21)*
CA1	*0.10*	*-0.26*
CA2	*-0.11*	*-0.17*
Dendate Gyrus	*0.06*	*-0.35*
Striatum	*-0.47**	*-0.28*
Motor Cortex	*-0.11*	*-0.38*
Visual Cortex	*-0.26*	*-0.36*
Cerebellum	*-0.26*	*-0.20*

** significant at the 0.05 level (2-tailed)*

Table 4

Correlation of mean percentage of GLUT1 and CD31 immunolabelled area and total distance run for various brain regions

Brain Region	*GLUT1 (n=21)*	*CD31 (n=21)*
CA1	*0.20*	*0.36*
CA2	*0.10*	*0.44**
Dendate Gyrus	*0.26*	*0.38*
Striatum	*0.44*	*0.55***
Motor Cortex	*0.05*	*0.14*
Visual Cortex	*0.42*	*0.00*
Cerebellum	*0.11*	*-0.05*

** significant at the 0.05 level (2-tailed)*
*** significant at the 0.01 level (2-tailed)*

Table 5

Western blot quantification of GLUT1 and β-tubulin protein expression (natural logarithm of the GLUT1 or β-tubulin and β-actin ratio ±S.E.M.) and F value for various brain regions

Brain Region	*GLUT1*				*β-tubulin*			
	Control (n=22)	*Sham (n=18)*	*Runners (n=17)*	*F*	*Control (n=22)*	*Sham (n=18)*	*Runners (n=17)*	*F*
Hippocampus	*0.04±0.06*	*0.30±0.08*	*0.29±0.11*	*3.53**	*-3.26±0.08*	*-3.15±0.10*	*-3.15±0.13*	*0.44*
Striatum	*-0.13±0.04*	*-0.04±0.09*	*0.12±0.08*	*3.32**	*-2.87±0.08*	*-2.80±0.08*	*-2.75±0.09*	*0.47*
Motor, somatosensory Cortex	*-0.05±0.07*	*0.22±0.06*	*0.11±0.11*	*2.14*	*-2.64±0.11*	*-2.65±0.10*	*-2.62±0.16*	*0.13*
Visual Cortex	*-0.18±0.07*	*-0.12±0.08*	*-0.16±0.09*	*0.18*	*-3.24±0.07*	*-3.13±0.08*	*-3.16±0.08*	*0.50*
Cerebellum (hemispheres)	*1.30±0.17*	*1.44±0.16*	*1.46±0.16*	*0.26*	*-4.01±0.15*	*-3.66±0.16*	*-3.80±0.16*	*1.13*
Cerebellum (vermis)	*1.22±0.09*	*1.29±0.18*	*1.37±0.12*	*0.31*	*-3.82±0.17*	*-3.93±0.19*	*-3.87±0.16*	*0.11*

** significant at the 0.05 level*

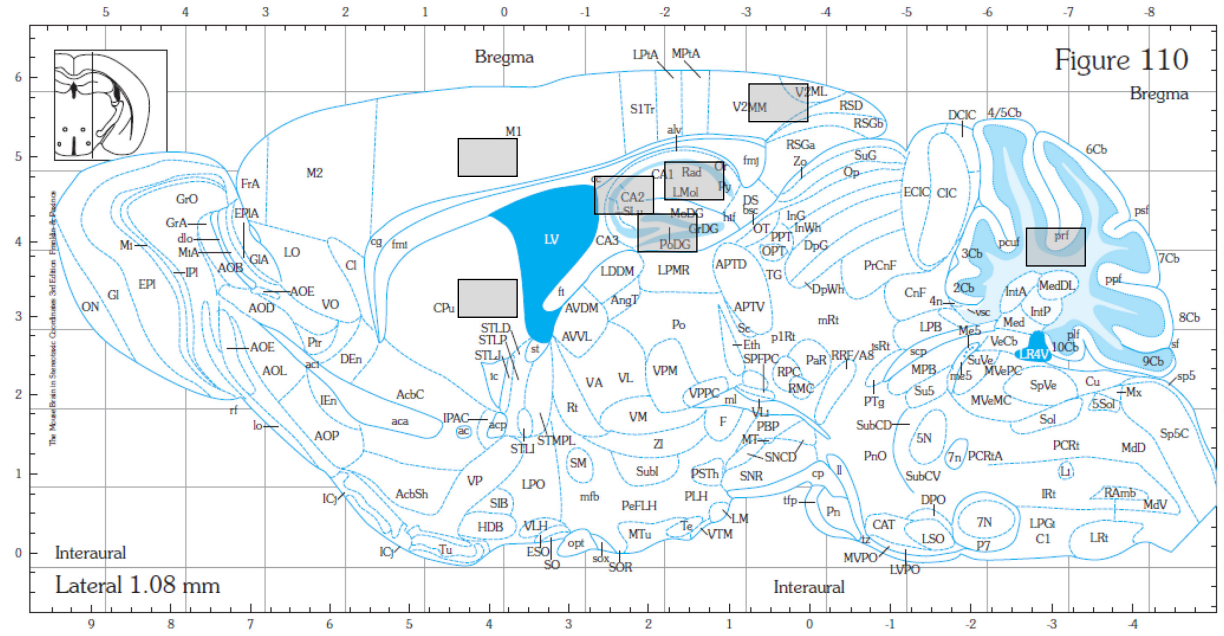

Figure 1. Localization of the sampled areas for GLUT1and CD31 immunoreactivity in the following brain regions: Motor cortex, visual cortex, striatum, hippocampus (CA1, CA2 and dentate gyrus) and cerebellum.

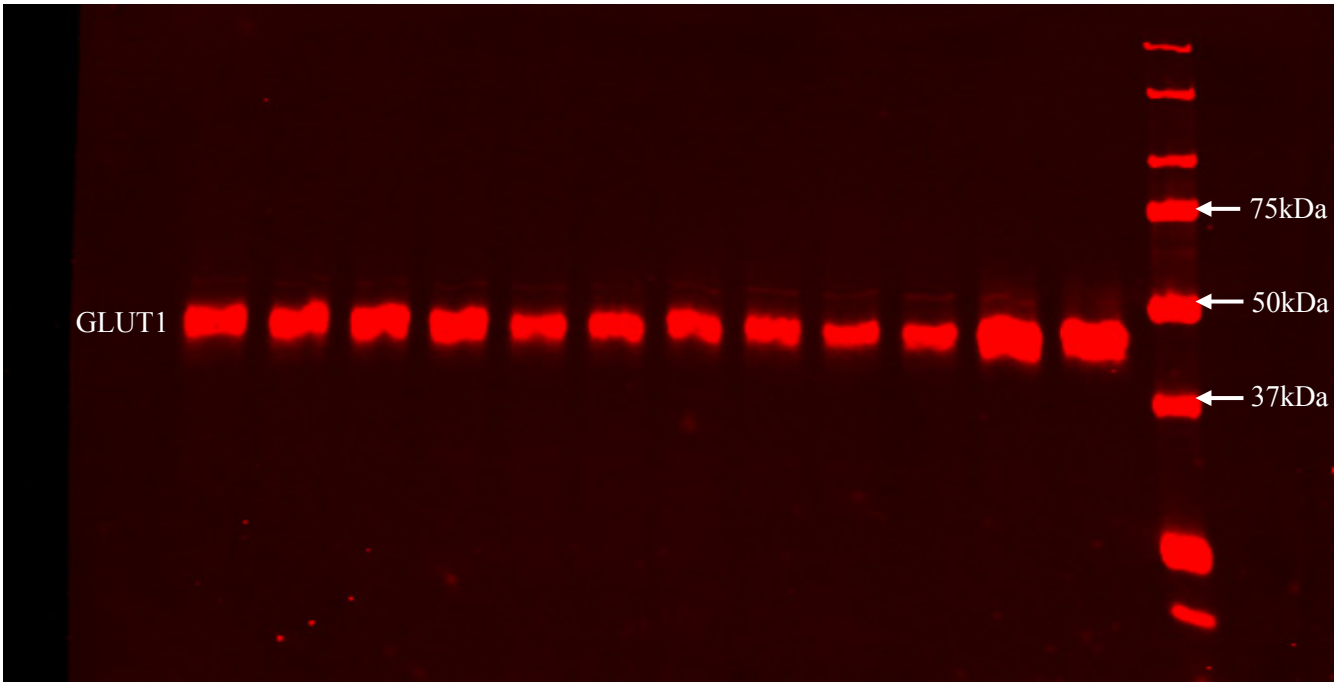

Figure 2. Example of western blot sample membrane scan in the IR700 channel. GLUT1 antibody is detected as a 45kDa band.

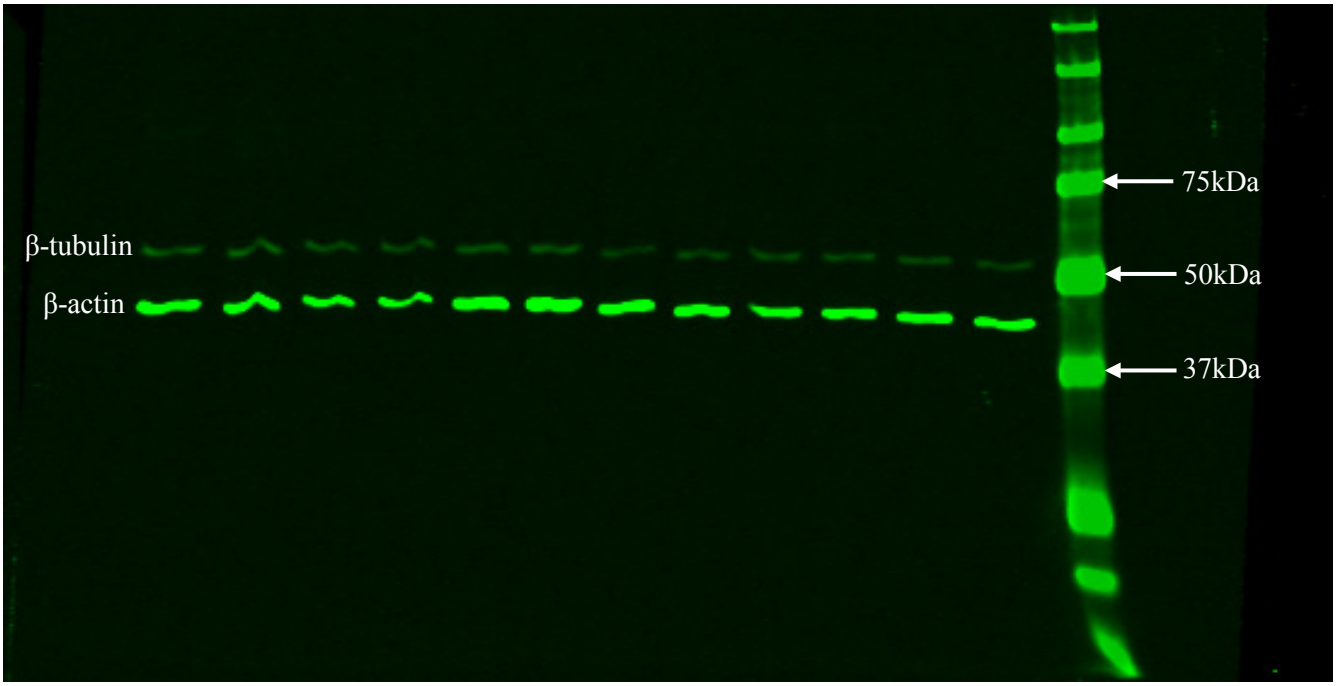

Figure 3: Example of western blot sample membrane scan on the IR800 channel. β-tubulin antibody is observed as a 55kDa band and β-actin antibody as a 42kDa band.

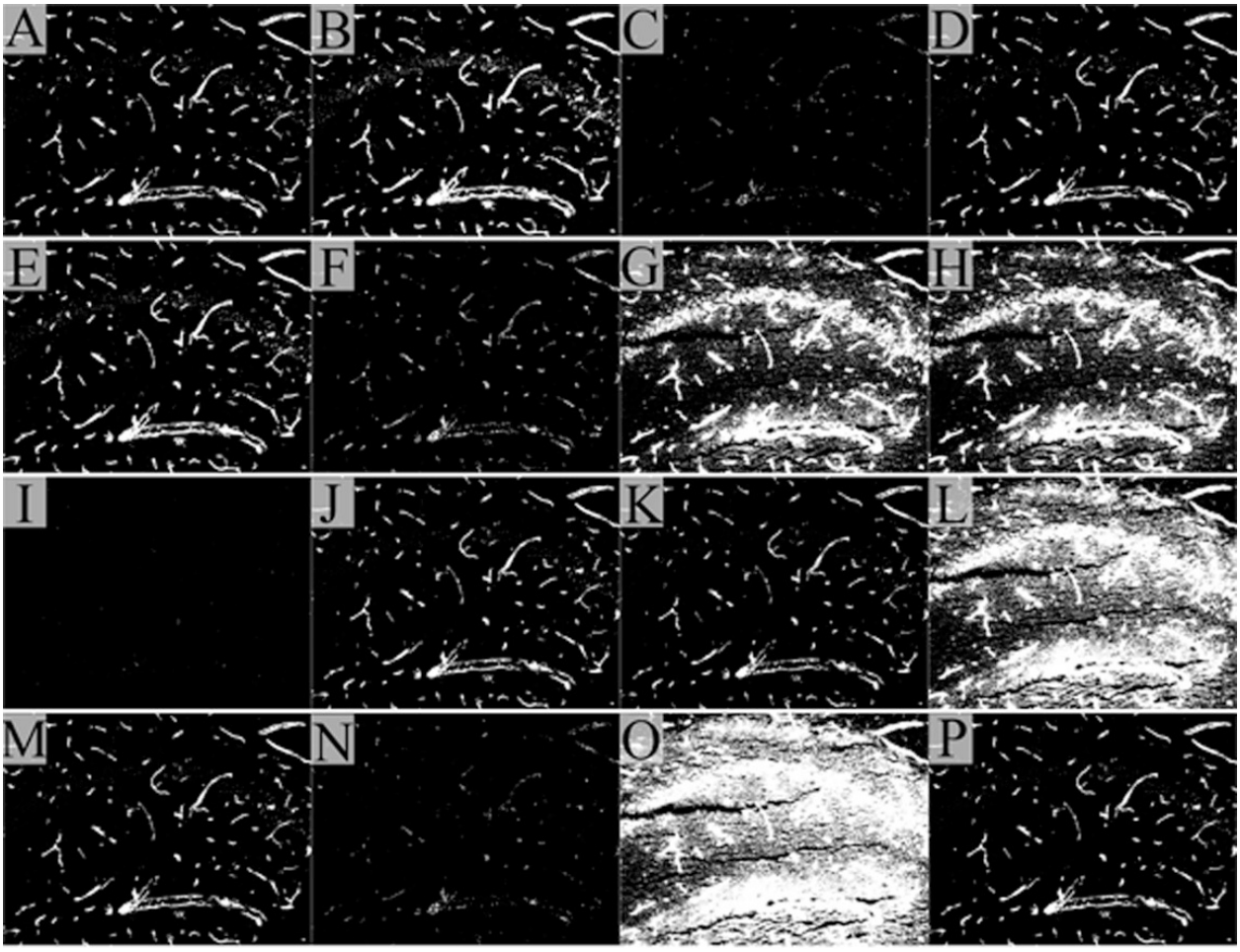

Figure 4. Results of 16 thresholding algorithms applied on the same image of GLUT1 immunolabelling in the hippocampal CA1 region. The thresholding methods were the following: ImgeJ default (A), Huang's fuzzy thresholding (B), Intermodes (C), IsoData (D), Li's minimum cross entropy (E), Kapur-Sahoo-Wong's MaxEntropy (F), Mean grey level (G), MinError (H), Minimum (I), Tsai's Moments-preserving (J), Otsu (K), Percentile (L), Renyi's Entropy (M), Shanbhag (N), Triangle (O), Yen's multilevel (P). All thresholding algorithms are included in the ImageJ software. Areas selected by the thresholding algorithm are shown in white.

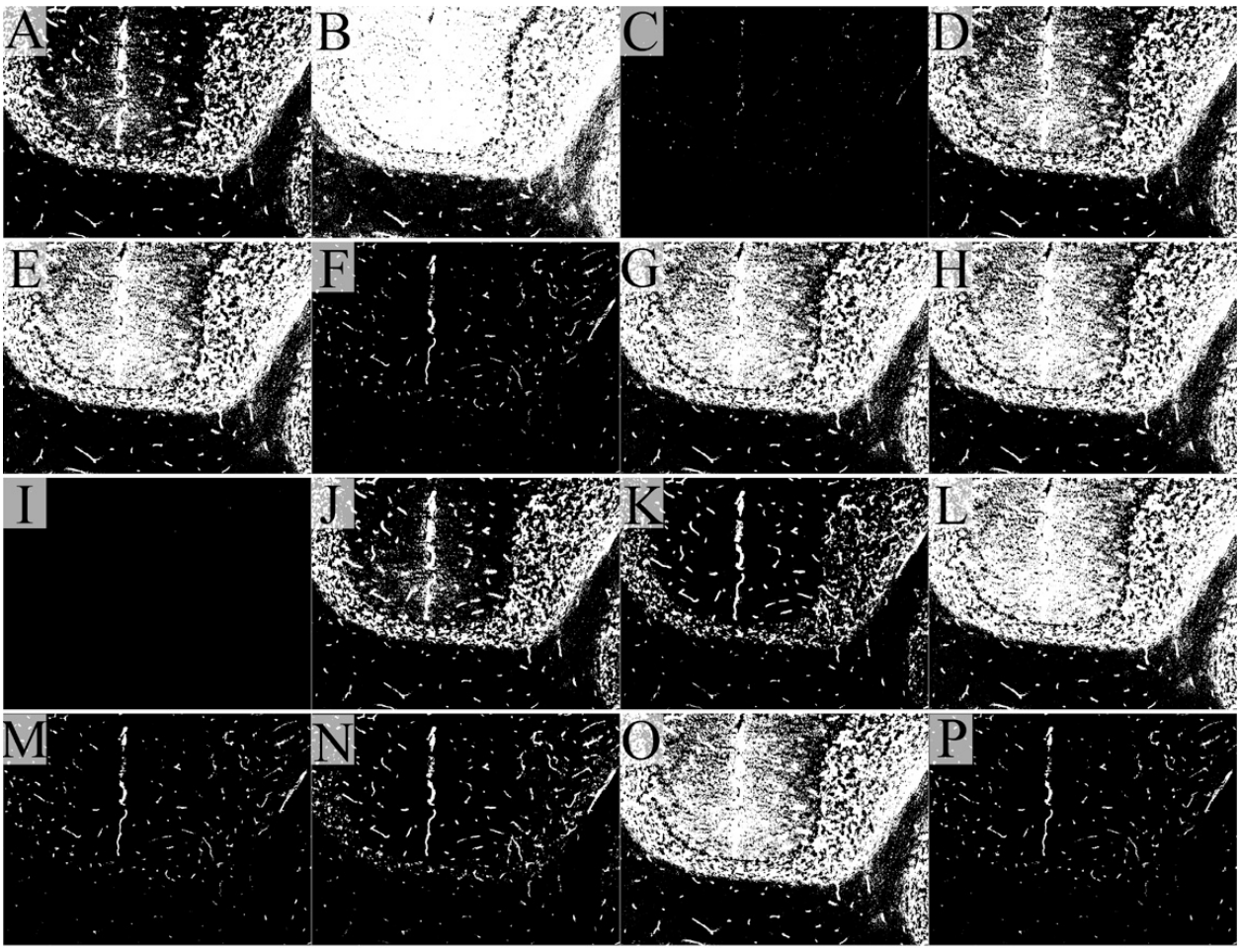

Figure 5: Results of 16 thresholding algorithms applied on the same image of GLUT1 immunolabelling in the cerebellum region. The thresholding methods used were the following: ImgeJ default (A), Huang's fuzzy thresholding (B), Intermodes (C), IsoData (D), Li's minimum cross entropy (E), Kapur-Sahoo-Wong's MaxEntropy (F), Mean grey level (G), MinError (H), Minimum (I), Tsai's Moments-preserving (J), Otsu (K), Percentile (L), Renyi's Entropy (M), Shanbhag (N), Triangle (O), Yen's multilevel (P). All thresholding algorithms are included in the ImageJ software. Areas selected by the thresholding algorithm are shown in white.

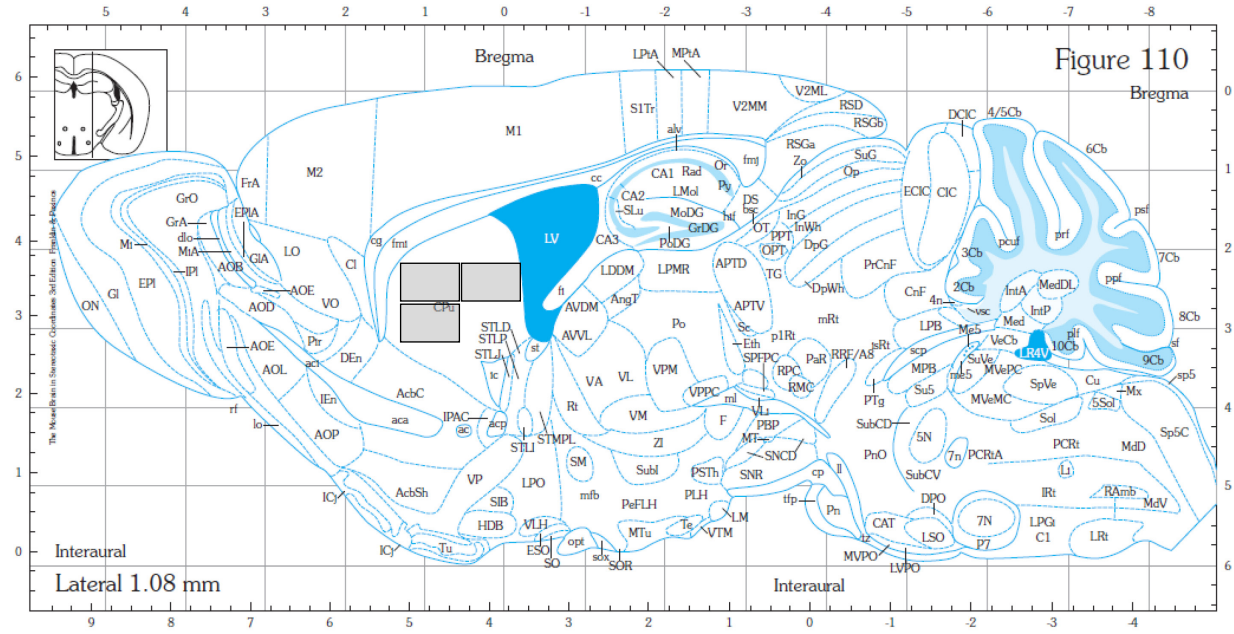

Figure 6. Localization of the brain areas used for the blood vessel diameter and density measurement.

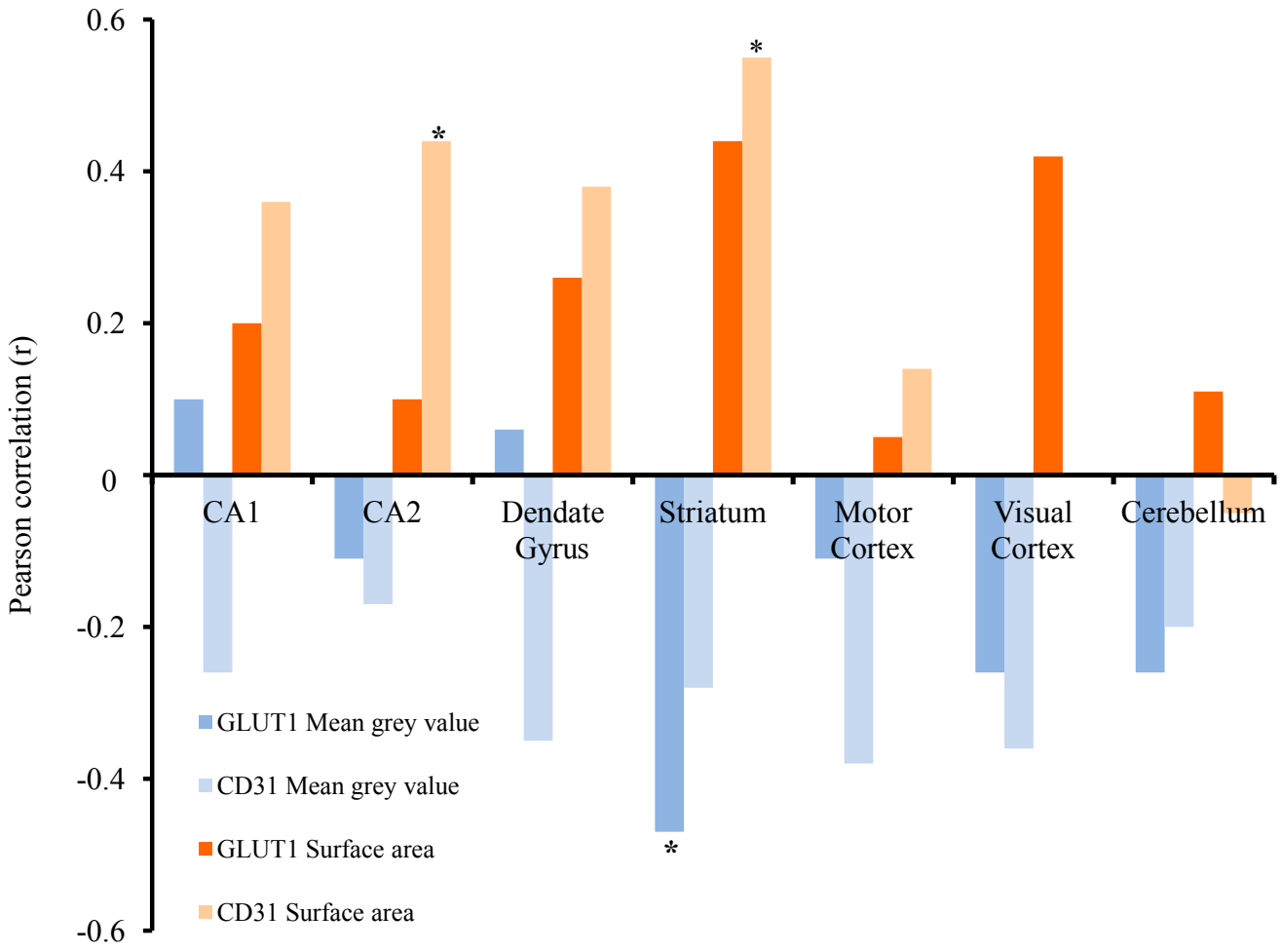

Figure 7. Pearson correlation between either the mean grey value or the surface area immunolabelled and the total distance run in 48h by mice in the experimental group.

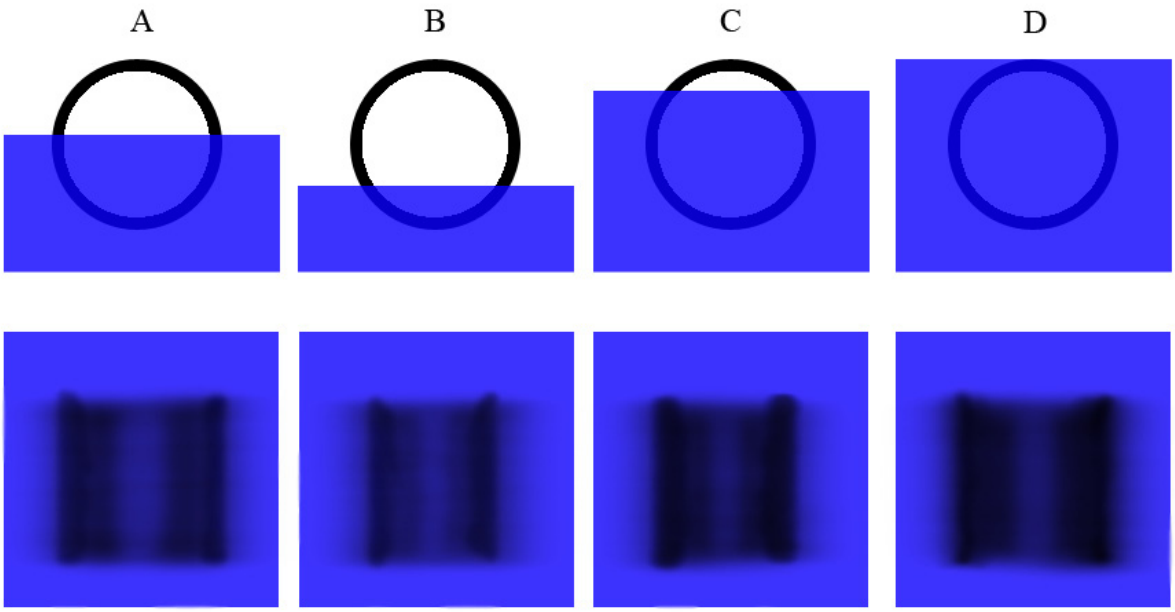

Figure 8. The figure shows how blood vessel diameter differs depending on the position on the brain slice. The upper figure shows the cross-sectional view of a blood vessel (black). The brain section is colored in blue. Since the section is thicker than most blood vessels we measured, this illustration shows where the blood vessel was cut off in the microscopic image presented in the lower panel. The lower panel presents the vessel as viewed with a bright field microscope. An estimate of the blood vessel diameter can be obtained in three of the four cases (A, C and D). However, only cases C and D provide a good and reliable estimate for diameter measurement since the total extent of the blood vessel can be observed by changing the focus.